Int. J. Electrochem. Sci., 13 **(2018)** 9583 – 9591, doi: 10.20964/2018.10.20

International Journal of
ELECTROCHEMICAL
SCIENCE
www.electrochemsci.org

Microstructure and Electrochemical Properties of Refractory Ta-Y_2O_3 and Ta-ZrO_2 Nanocomposites

M. Sopata, G. Adamek, J. Jakubowicz[*]

Poznan University of Technology, Institute of Materials Science and Engineering, Jana Pawla II, 24, 61-138 Poznan, Poland
[*]E-mail: jaroslaw.jakubowicz@put.poznan.pl

Received: 18 May 2018 / *Accepted:* 9 July 2018 / *Published:* 1 September 2018

The refractory tantalum-ceramic oxide nanocomposites were made using mechanical alloying. The tantalum powder was synthesized together with Y_2O_3 or ZrO_2 powders in the concentration of 5, 10, 20 and 40 wt.%. The nanocomposite powders were hot-pressed using the pulse plasma sintering mode. To achieve good sample integrity, the hot pressing at the temperature of 1300-1500^oC was done. The nanocomposites had a crystallite size below 100 nm. The corrosion resistance was measured using the potentiodynamic mode in the Ringer's electrolyte. The increase of oxide ceramic phase content leads to increased corrosion resistance. Best corrosion resistance is exhibited by the Ta-20Y_2O_3 and Ta-20ZrO_2 composites with the corrosion current density of up to 4 orders of magnitude lower than for pure nanocrystalline tantalum.

Keywords: Tantalum-ceramic oxide nanocomposites; mechanical alloying; corrosion resistance

1. INTRODUCTION

Tantalum belongs to a group of elements of the highest corrosion resistance, higher than titanium or stainless steel [1]. Tantalum is corrosion resistant in concentrated and hot acidic environments, which results in the formation of a passive Ta_2O_5 oxide film. As the pure metallic element its mechanical strength is relatively low, however corrosion resistance is very high. Introduction of the alloying elements raises its strength, but the corrosion resistance may be lower [2]. Tantalum and its alloys as a refractory material have found specific applications in chemical, mechanical and aeronautical industry. The last decade saw an increased trend to use composite materials, mainly based on plastics such as carbon fiber reinforced epoxy resins. The very hard working conditions in many applications impose an application of new advanced metallic or ceramic-

based composites. Many alloys can be improved in terms of resistance to wear, corrosion and mechanical properties through the introduction of ceramic reinforced phases [3-6]. Similarly, the properties of ceramics can be improved through an introduction of other reinforced ceramic phases [7]. In the case of the refractory metals and alloys [8], their properties such as mechanical strength, hardness, wear resistance, creep or corrosion resistance can be improved through the introduction of reinforced refractory ceramic phases to their microstructure [9-11]. For high-temperature application the oxide ceramic is the most promising due to its resistance to decomposition in oxidative atmosphere at elevated temperatures. The behavior of carbides or nitrides may be different than that of oxides (for example they can decompose to oxides such as $SiC + 2O_2 \rightarrow SiO_2 + CO_2$, or $Si_3N_4 + 3O_2 \rightarrow 3SiO_2 + 2N_2$), however both (as oxides) will improve the mechanical properties at room and moderate temperatures [12].

New possibilities for the improvement of structural materials are the results of the advancement of nanomaterials. For nanomaterials the strength is improved according to the Hall–Petch equation, where the grain size reduction results in a mechanical strength improvement [13]. The main downside of nanomaterials having a high volume of the grain boundaries is lower corrosion resistance in comparison to their microcrystalline counterparts [14] as well as low-temperature stability that lead to grain growth. For that reason new solutions to this problem need to be found. Our proposal in the case of nanocrystalline tantalum is to make composites with reinforced refractory ceramics of higher corrosion resistance. In our previous work the authors showed the formation and mechanical properties of the Ta-ceramic nanocomposites [15]. In this work the authors show the corrosion properties of the Ta-ceramic oxides nanocomposites, where Y_2O_3 and ZrO_2 are the ceramic reinforcing phases. The nanocomposites were produced in the mechanical alloying process and the obtained powders were hot-pressed in the Pulse Plasma Sintering (PPS) mode. In this work the authors focus on the electrochemical properties of the nanocomposites while the structural results are shown only as examples for better understanding of the paper, because more detailed structural and mechanical properties of these composites have been shown in [15].

2. MATERIALS AND METHODS

In this work Ta-xY_2O_3 and Ta-xZrO_2 nanocomposites containing x = 5, 10, 20 and 40 wt.% of the ceramic phase were synthesized (marked as Ta-xY_2O_3 and Ta-xZrO_2, where x is 5, 10, 20 or 40 in wt.%). The tantalum-based nanocomposite powders were produced by mechanical alloying (MA). For the MA process the authors used a mixture of the tantalum powder (<44 μm; purity >99.97%; Alfa Aesar) with the ceramic powder: Y_2O_3 (<50nm; purity >99.9%; Sigma-Aldrich) and ZrO_2 (0.1-2μm; stabilized with 5.4% of Y_2O_3; Goodfellow). A mixture of 5.5g of the powders was blended and milled for 48h in the SPEX 8000M Mixer/Mill (Spex SamplePrep) according to the procedure described elsewhere [15]. At all the processing stages (powder handling, milling) argon atmosphere was applied.

The as-milled powders were axially hot-pressed at vacuum using graphite die and graphite movable punches. The pressure of the punches directed at the powder was 50 MPa. In the consolidation process, the Pulse Plasma Sintering mode (PPS) was applied. The experimental details

related to consolidation have been described elsewhere [15, 16]. The pressing temperature was fixed at 1300^{o}C and 1500^{o}C. Higher temperature was applied for higher ceramic phase content to achieve full sample integrity. Higher ceramic content in the composite needs a higher temperature for full consolidation, yet not too high, as it would result in excess grain growth. The time of sintering at a constant temperature was 5 s (the temperature rises up till it reaches the end value for 2-2.5min). The hot-pressed bulk samples were 8 mm in diameter and 4 mm in height.

The structure was analyzed using XRD (Empyrean; Panalytical) equipped with ICDD-JCPDS database. The crystallite size of the nanocomposites was estimated by the Williamson-Hall (W-H) method. The nanocomposite powders as well as the thin foil of the hot-pressed samples were analyzed using TEM (CM20 Super Twin; Philips).

The corrosion resistance was measured on hot-pressed samples using a Solartron 1285 Potentiostat (Solartron Analytical). The measurements started after OCP (open-circuit-potential) stabilization at a constant value and the polarization curves were recorded from −0.5V up to 2.5V vs. OCP. The scan rate was 0.5 mV/s. The graphite and Ag/AgCl were used as the counter and reference electrodes, respectively. A standard EG&G electrochemical cell (Princeton Applied Research) was used. The corrosion resistance was measured in the mixed and nitrogen purged Ringer's electrolyte containing chloride ions (147.2 mmol$\cdot$ l^{-1} Na^{+}, 4.0 mmol$\cdot$ l^{-1} K^{+}, 2.2 mmol$\cdot$ l^{-1} Ca^{2+}, 155.7 mmol$\cdot$ l^{-1} Cl^{-}). For the corrosion tests the bulk samples were grinded on sandpaper up to 1000 grit and polished in Al_2O_3 suspension to obtain a mirror-like surface of low roughness. As the reference materials, the authors used hot pressed micro- and nanocrystalline Ta.

3. RESULTS AND DISCUSSION

The tantalum-ceramic oxide nanocomposites were made using mechanical alloying and hot pressing. The examples of structural data for the considered nanocomposites have been presented in Fig. 1 showing the XRD spectra for pure Ta (a), Y_2O_3 (b) and ZrO_2 (c) powders as well as the spectra for example Ta-20Y_2O_3 (d) and Ta-20ZrO_2 (e) nanocomposites after mechanical alloying and further consolidation (f) and (g), respectively. The mechanical alloying results in the formation of nanocomposites with main broad peaks on the XRD spectra with their position corresponding to Tantalum. The peaks of Y_2O_3 and ZrO_2 in these nanocomposites are invisible because they are masked by the broad peaks of tantalum up to 20% of the oxide content [15]. The broad peaks also indicate the nanostructure formation. The hot pressing at an elevated temperature results in a reaction between the composite elements. The composite powders also react partially with the graphite matrix, which results in the formation of tantalum carbides (TaC, Ta_2C). Finally, the bulk composites obtain a complex structure with the main Ta, and Y_2O_3 or ZrO_2 phases as well as other minor phases (Y_3TaO_7, Ta_2O_5). The crystallite size was obtained based on the XRD spectra using the W-H plots (Fig. 2a,b). The mechanical alloying carried out at a room temperature leads to the formation of a metal-ceramic composite powder mixture [15]. The dynamic milling in the MA process leads to a significant Ta powders cold strengthening, increases their brittleness and finally the reduction of the Ta crystallite size. The high energy of impacts among the milling balls leads to a cracking through the brittle

ceramic particles and their refinement (Fig. 2c). The hot pressing increases the crystallite size (Fig. 2d).

The example TEM images (Fig. 3) show the Ta-20Y_2O_3 nanocomposite after mechanical alloying (a) and after hot pressing (b). The exemplary grains have been indicated. The mechanical alloying results in a uniform distribution of metal and ceramic particles. The Y_2O_3 nanoparticles after MA are smaller in comparison to the Ta nanoparticles in the powder mixture (a). The hot pressing increases the grain size and, for the presented Ta-20Y_2O_3 nanocomposite the average grain size is 75 nm, whereas the full grain size distribution is in the range of 25-150 nm (larger for the Ta grains). In all composites the average grain size is below 100 nm [15]. The data measured by TEM are roughly consistent with those calculated using the W-H method.

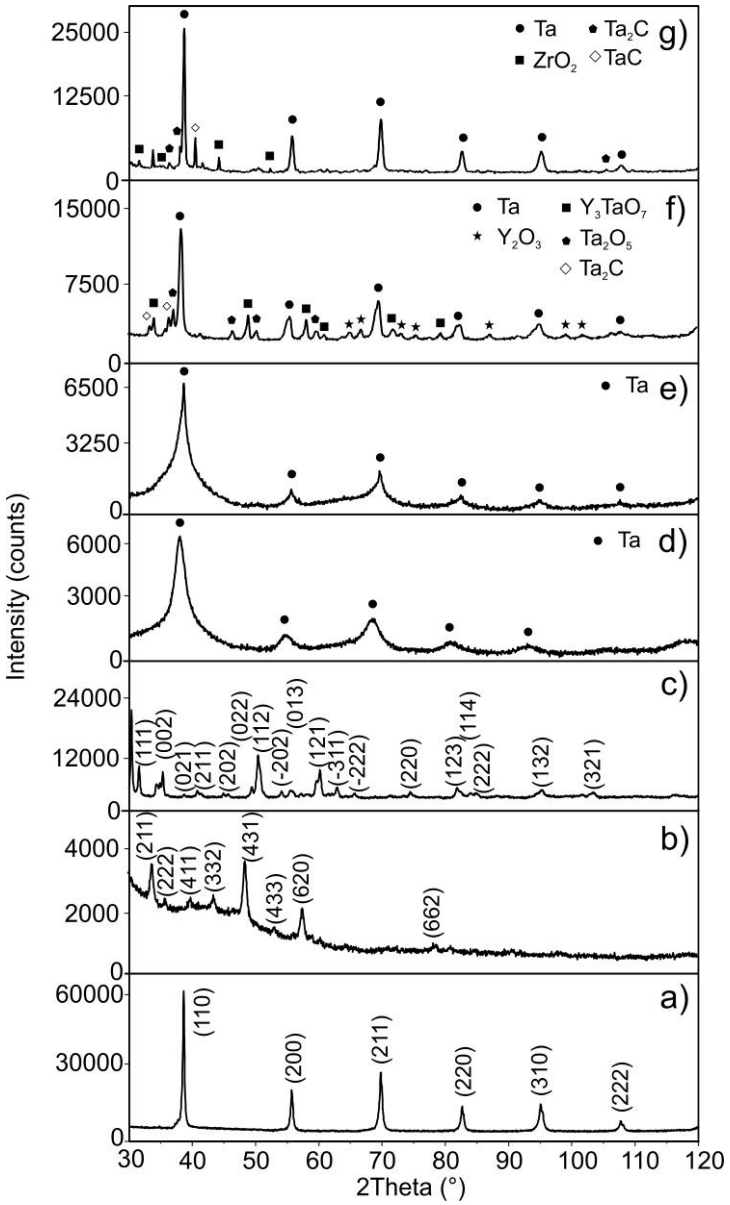

Figure 1. XRD of pure Ta (a), Y_2O_3 (b) and ZrO_2 (c) powders and example Ta-20Y_2O_3 (d) and Ta-20ZrO_2 (e) nanocomposites after mechanical alloying and after consolidation (f) and (g), respectively

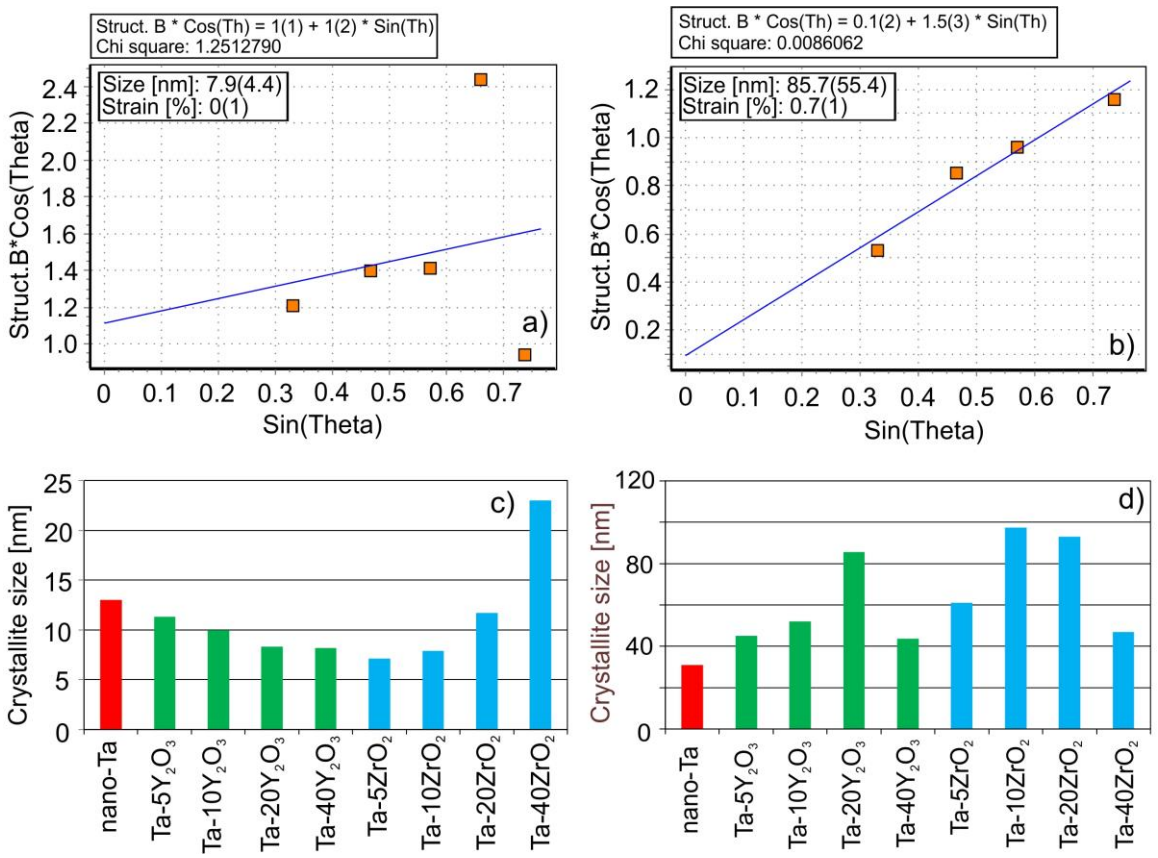

Figure 2. Example Williamson-Hall plot for the Ta-20Y_2O_3 nanocomposite after MA (a) and after hot pressing (b), and average crystallite size of the Ta-ceramic nanocomposites after MA (c) and after hot pressing (d)

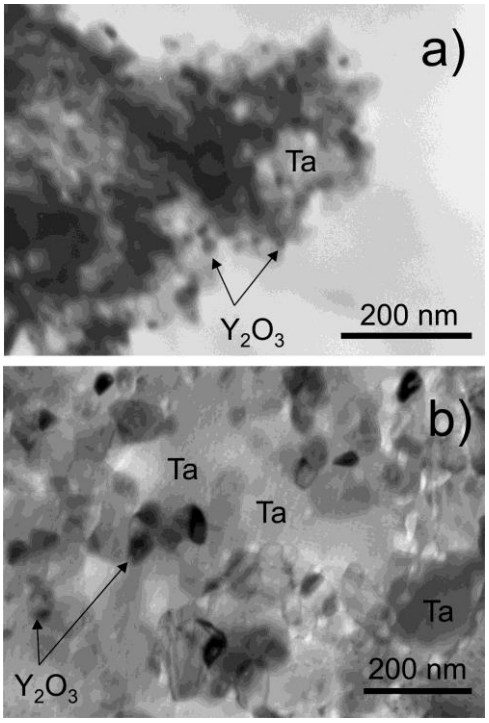

Figure 3. TEM images of the Ta-20Y_2O_3 nanocomposite after MA (a) and after hot pressing (b)

The corrosion resistance was measured in the Ringer's electrolyte. First, the samples were kept at OCP until they stabilized (Fig. 4). Later, the samples were polarized from the cathodic to the anodic potential range (Figs. 5, 6). The current density and values of potential read from the polarization curves have been summarized in Table 1.

The OCP is a stationary potential that changes in time and roughly shows the material tendency to corrode. The OCP changes during sample soaking in the electrolyte and provides information on how stable the passive oxide layer is (Fig. 4). The highest negative OCP value indicates the composites with the highest content of the ceramic oxide and a relatively high negative OCP also points to microcrystalline tantalum. The OCP shifts with time to a more positive value indicating a tendency for passivation and thickening of the native oxide layer. For pure nanocrystalline tantalum the OCP slightly shifts to a negative value and in this case a stable passive layer does not form.

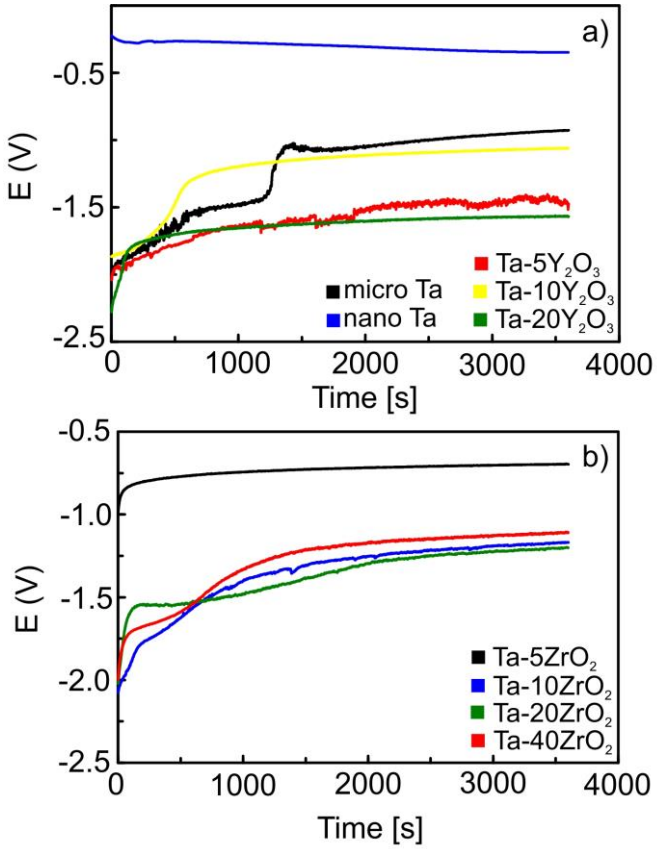

Figure 4. OCP as a function of time in the Ringer's electrolyte for the Ta-Y_2O_3 (a) and Ta-ZrO_2 (b) nanocomposites; for comparison data for nano- and microcrystalline Ta have been included in (a)

The polarization curves for the nanocomposites have been presented in Fig. 5 and Fig. 6. The results for reference micro- and nanocrystalline pure Ta have been shown in the authors' previous work [16]. For better clarity and comparison to the reference material the authors repeated the data for pure Ta only from their previous work [16]. Pure microcrystalline Ta as a reference material has very good corrosion resistance. The corrosion current density, which indicates the corrosion resistance is very low (I_{corr} = $3.108 \cdot 10^{-8}$ A/cm^2). Nanocrystalline Ta has a significantly higher corrosion current

density (I_{corr} = 1.198·10^{-5} A/cm^2). Large volume of the grain boundaries results in deterioration of the corrosion resistance.

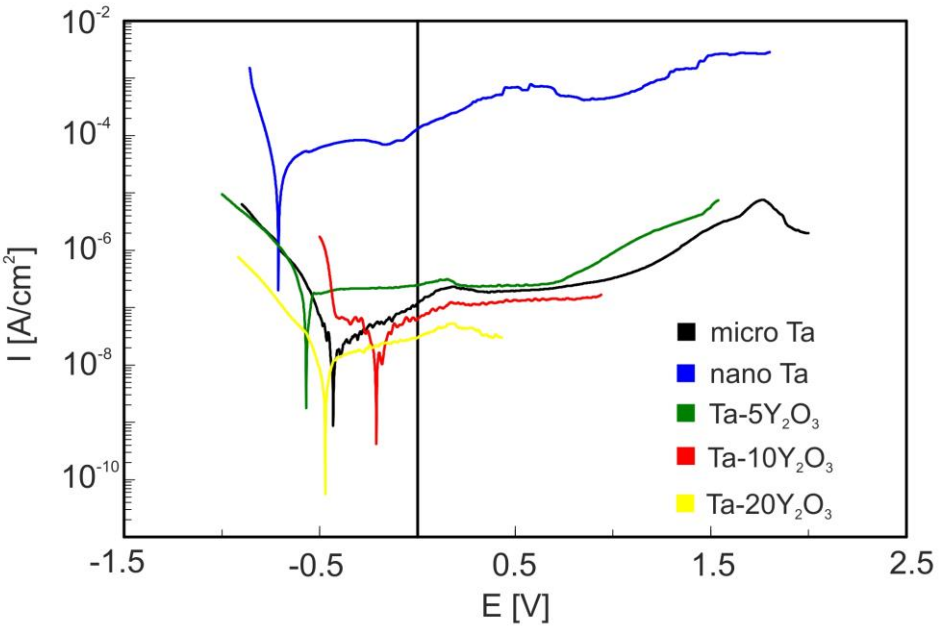

Figure 5. Polarization curves in the Ringer's electrolyte of the microcrystalline Ta, nanocrystalline Ta and Ta-xY_2O_3 nanocomposites (x=5, 10, 20 wt.%)

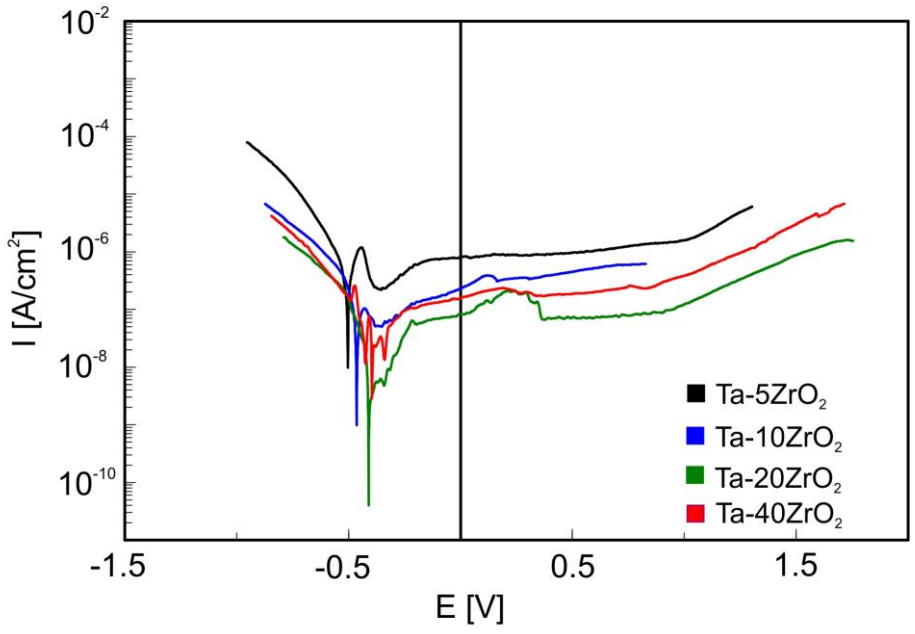

Figure 6. Polarization curves in the Ringer's electrolyte of the Ta-xZrO_2 (x=5, 10, 20, 40 wt.%) nanocomposites

As was presented in the authors' previous work [16], the modification of the chemical composition of Ta through an introduction of Nb, Mo, and W significantly improves the corrosion resistance of the nanocrystalline alloys in comparison to pure nanocrystalline Ta. In this work, the

authors focused on the Ta nanocomposites modified by ceramic oxide particles. It was expected that the oxides that have high energy of oxide formation improve the corrosion resistance of the composites in comparison to pure Ta whose energy is negative. The polarization curves were measured for all the investigated composites except of Ta-40%Y_2O_3. The very high content of the insulating oxide phase in the composite (here 40% of Y_2O_3) results in its poor electrical conductivity, which makes impossible to measure the polarization curve of this material. However it is expected that this material possesses a high corrosion resistance. The Ta-5Y_2O_3 shows a wide plateau in the passive range, however an increase in the Y_2O_3 content leads to a reduced corrosion current density and current density in the passive range. The comparable tendency was observed for the Ta-ZrO_2 composites. For Ta-5ZrO_2 the plateau was wide and the corrosion current density was the lowest for Ta-20ZrO_2. Based on the polarization curves the critical currents and potentials were measured and shown in Table 1.

The values of the Tafel slopes indicate the tendency to corrosion resistance of the materials. The Tafel slopes theoretical values of 120, 40 and 30 mV are observed for the Volmer, Heyrovsky and Tafel determining rate steps. For our experimental polarization curves the kinetics of reactions is complex and its hardly to fit to one theoretical model. The anodic values of Tafel slope b_a are higher in comparison to cathodic Tafel slope b_c, which means that materials have tendency toward passivation (Tab. 1). When the b_c would be higher than b_a, the materials will have tendency to corrode [17].

In the nanomaterials the large volume of the grain boundaries results in materials having a higher energy, which unfortunately deteriorates the corrosion resistance [14]. On the other hand, the grain boundaries provide a higher density of the nucleation sites for the formation of a passive film [18], which in some cases could lead to an improvement of the corrosion resistance.

Table 1. Corrosion current density I_{corr}, corrosion potential E_{corr}, passivation potential E_p, passivation current density I_{cp} as well as Tafel cathodic slope b_c and Tafel anodic slope b_a of the investigated hot-pressed Ta-ceramic nanocomposites; data for pure Ta for comparison [16]

sample	I_{corr} [A/cm^2]	E_{corr} [V]	E_p [V]	I_{cp} [A/cm^2]	b_c [mV]	b_a [mV]
micro-Ta	$3.108\cdot10^{-8}$	-0.398	0.135	$6.166\cdot10^{-7}$	-92.6	273.4
nano-Ta	$1.198\cdot10^{-5}$	-0.711	-0.318	$1.298\cdot10^{-4}$	-63.9	137.9
nanocomposites:						
Ta-5Y_2O_3	$1.433\cdot10^{-7}$	-0.573	0.160	$3.096\cdot10^{-7}$	-64.6	53.2
Ta-10Y_2O_3	$1.605\cdot10^{-8}$	-0.209	0.170	$1.235\cdot10^{-7}$	-95.6	135.5
Ta-20Y_2O_3	$4.064\cdot10^{-9}$	-0.470	0.175	$5.311\cdot10^{-8}$	-114.9	120.9
Ta-40Y_2O_3	–	–	–	–	–	–
Ta-5ZrO_2	$2.159\cdot10^{-7}$	-0.504	-0.439	$1.197\cdot10^{-6}$	-62.0	75.3
Ta-10ZrO_2	$4.185\cdot10^{-8}$	-0.464	-0.429	$1.045\cdot10^{-7}$	-52.9	54.7
Ta-20ZrO_2	$4.464\cdot10^{-9}$	-0.358	-0.214	–	-49.0	163.4
Ta-40ZrO_2	$3.720\cdot10^{-8}$	-0.414	0.190	$2.352\cdot10^{-7}$	-44.9	190.9

High mechanical properties of the investigated composites were presented in [15] while this work also shows that the nanocomposites have a very high corrosion resistance. The materials can find applications in heavy duty working conditions (friction wear and corrosion environments).

4. CONCLUSIONS

In this work the authors discussed the corrosion resistance of the Ta-xY_2O_3 and Ta-xZrO_2 nanocomposites containing x = 5, 10, 20 and 40 wt.% of the ceramic phase. The nanocomposites were prepared using mechanical alloying and subsequent hot pressing. The authors have observed that the introduction of oxides results in an extraordinarily improved corrosion resistance in all composites compared to pure nanocrystalline Ta. The introduction of oxides ensures comparable or even better properties than pure microcrystalline Ta. The best corrosion resistance was exhibited by composites having 20 and 40% content of oxide, yet for the Ta-40Y_2O_3 nanocomposite due to its insulating properties it was impossible to measure the polarization curve.

ACKNOWLEDGMENTS
The work has been financed by National Science Centre, Poland under project identification DEC-2015/19/B/ST5/02595

References

1. A. Robin, *Int. J. Refract. Met. Hard Mater*., 15 (1997) 317.
2. S.M. Cardonnne, P. Kumar, C.A. Michaluk and H.D. Schwartz, *Int. J. Refract. Met. Hard. Mater*., 13 (1995) 187.
3. P. Agrawal and C.T. Sun, *Compos. Sci. Techn*., 64 (2004) 1167.
4. F. Scherm, R. Völkl, A. Neubrand, F. Bosbach and U. Glatzel, *Mater. Sci. Eng. A*, 527 (2010) 1260.
5. K. Niespodziana, K. Jurczyk and M. Jurczyk, *Adv. Mater. Sci.* 14 (2007) 102.
6. P. Siwak and D. Garbiec, *Trans. Nonferrous Met. Soc. China*, 26 (2016) 2641.
7. T. Ohji, *Scripta Mater*., 44 (2001) 2083.
8. R. Morales, R.E. Aune, O. Grinder and S. Seetharaman, *JOM*, 55 (2003) 20.
9. X. Sun, W. Han, Q. Liu, P. Hu and Ch. Hong, *Mater. Design*, 31 (2010) 4427.
10. J.-H. Kim, M. Seo and S. Kang, *Int. J. Refract. Met. Hard Mater.*, 35 (2012) 49.
11. O. Gaballa, B.A. Cook and A.M. Russell, *Int. J. Refract. Met. Hard Mater.*, 41 (2013) 293.
12. K. Komeya and M. Matsui, High Temperature Engineering Ceramics, in *Materials Science and Technology*, (2006) 517.
13. N. Hansen, *Scripta Mater.*, 51 (2004) 801.
14. P. Herrasti, C. Ponce de León and F.C. Walsh, *Rev. Metal.*, 48 (2012) 377.
15. J. Jakubowicz, M. Sopata, G. Adamek, P. Siwak, and T. Kachlicki, *Adv. Mat. Sci. Eng*., 2018 (2018) 2085368.
16. J. Jakubowicz, G. Adamek, M. Sopata, J.K. Koper, T. Kachlicki and M. Jarzebski, *Int. J. Electrochem. Sci*., 13 (2018) 1956.
17. D. Mareci, G. Ungureanu, D.M. Aelenei and J.C. Mirza Rosca, *Mat. Corr*., 58 (2007) 848.
18. L. Jinlong, *J. Mat. Sci. Techn*., 34 (2018) 1685.